ACS APPLIED ENERGY MATERIALS

www.acsaem.org Article

Synergy of Charge Storage Properties of CuO and Polypyrrole in Composite CuO-Polypyrrole Electrodes for Asymmetric Supercapacitor Devices

Mahmoud Awad, Mohamed Nawwar, and Igor Zhitomirsky*

Cite This: ACS Appl. Energy Mater. 2024, 7, 5572−5581 Read Online

ACCESS | Metrics & More | Article Recommendations | Supporting Information

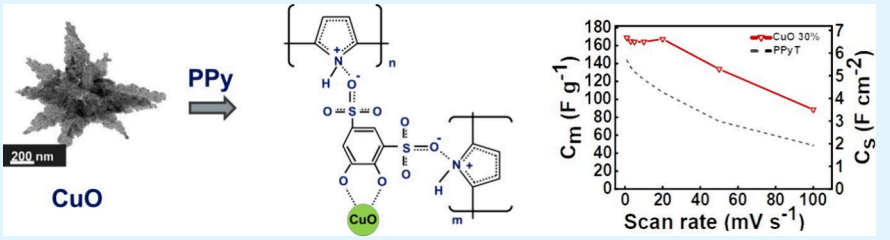

ABSTRACT: This investigation is motivated by interest in the redox properties of CuO for energy storage in supercapacitors and in the fascinating effects of charge transfer in conductive polymer−metal oxide composites on their physical and chemical properties. Various challenges are successfully addressed, such as efficient utilization of capacitive properties of charge storage materials in high active mass loading electrodes; understanding charge storage mechanisms at different electrode potentials; fabrication of anodes with high areal capacitance, which can match the capacitance of advanced cathodes; and fabrication of advanced asymmetric supercapacitor devices with high specific energy. CuO nanoparticles are prepared by hydrothermal synthesis and polypyrrole (PPy) particles are prepared by chemical polymerization for the fabrication of CuO and composite PPy-CuO anodes. An important finding is the synergistic effect of capacitive properties of PPy and CuO, which facilitates the fabrication of anodes with a record high capacitance of 7 F cm^{-2} in a 0.5 M Na_2SO_4 electrolyte. The capacitance, impedance, and charge transfer resistance of the composites are optimized by investigating electrodes with different PPy contents. The superior behavior of the composites is linked to the enhanced charge transfer, which results in a low impedance and reduced charge transfer resistance. The composite electrodes show good capacitance retention at fast charge−discharge rates and good cyclic stability. The asymmetric supercapacitor devices show high capacitance of 2.76 F cm^{-2} in a voltage window of 1.5 V, high energy density of 10.83 Wh kg^{-1}, and good cyclic stability.

KEYWORDS: *copper oxide, polypyrrole, composite, high active mass, supercapacitor, charge transfer*

INTRODUCTION

Oxides of transition elements, such as Fe, Mn, Co, Ni, and Cu, are promising for energy storage in supercapacitor devices.[1−4] The charge storage properties of Fe_3O_4, γ-Fe_2O_3, MnO_2, Mn_3O_4, Co_3O_4, NiO, and CuO are related to changes of the valence of the corresponding metal ions in chemical redox reactions.[1,4] CuO offers benefits for supercapacitor applications due to its low cost and chemical stability. Cyclic voltammetry studies[5,6] of CuO showed reduction of Cu^{2+} to Cu^{+} and Cu^{+} to Cu. This provides a platform for the application of CuO in anodes of supercapacitors.[7] However, the charge storage properties of CuO are not well understood. The electrochemical mechanisms based on the reduction of Cu^{2+} ions cannot explain the capacitive behavior of CuO at positive electrode potentials.[8−10]

Many investigations focused on CuO films with relatively low mass.[8,11−13] Electrochemical testing was performed in different electrolytes, such as KOH,[8−11] Na_2SO_4,[12,14] ionic liquids,[15] and other electrolytes.[16] Various dopants were investigated for the fabrication of doped CuO electrodes with enhanced properties.[17,18] The capacitance of the electrodes can be boosted under the influence of illumination, which generates electrons and holes in the semiconducting CuO material[19] and facilitates charge transport. Investigations of CuO electrodes showed a relatively high electrical resistance.[8,9] An areal capacitance of 120 mF cm^{-2} was reported for CuO electrodes in a Na_2SO_4 electrolyte.[14] Cu/CuO nanorod array electrodes showed an areal capacitance of 1.674 F cm^{-2} in a KOH electrolyte.[10] It should be noted that significantly higher capacitances are necessary for CuO applications in anodes of supercapacitor devices. The areal capacitance of the anodes

Received: May 10, 2024
Revised: June 13, 2024
Accepted: June 18, 2024
Published: June 25, 2024

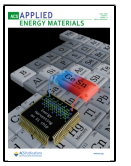

https://doi.org/10.1021/acsaem.4c01204
ACS Appl. Energy Mater. 2024, 7, 5572−5581

must be matched with the areal capacitance of advanced Mn_3O_4 or MnO_2 cathodes, which showed high capacitances at the level of ~6−8 F cm^{-2} in a Na_2SO_4 electrolyte.[1,20,21] Therefore, the low areal capacitance of CuO anodes is a limiting factor for the applications of this material in asymmetric supercapacitors. It should be noted that aqueous asymmetric supercapacitors are environmentally friendly and offer advantages of enlarged voltage window and high energy and power density compared to aqueous symmetric supercapacitors.[22−25]

It has previously been shown that composites of CuO and conductive polymers, such as polypyrrole (PPy), offer interesting effects, which provide a platform for advanced energy storage applications in supercapacitors and batteries.[26−29] The electrochemical studies of composite electrodes showed good charge storage properties due to enhanced conductivity and reduced volume changes during charge and discharge. CuO-PPy nanowire array supercapacitor electrodes showed a capacitance of 1080 mF cm^{-2} in a KOH electrolyte.[30] However, PPy showed rapid degradation of properties in alkaline electrolytes.[31] Other investigations of CuO-PPy composites focused on supercapacitors with a low active mass and reported high gravimetric and volumetric capacitance.[32−34] The addition of PPy to CuO resulted in enhanced conductivity and increased capacitance. However, there is a need to develop highly active mass electrodes with high areal capacitance for practical applications. However, the poor electrochemical performance of such electrodes at high active mass loading is a bottleneck hindering their applications in supercapacitor devices.

The goal of this investigation was the fabrication of CuO and CuO-PPy electrodes for energy storage in asymmetric supercapacitors. It addressed the need for a better understanding of the charge storage mechanism. Motivated by the high interest in practical applications of CuO-based electrodes, we fabricated electrodes with a high active mass loading of 40 mg cm^{-2}. Despite the many reports in the literature on the drastic reduction of gravimetric capacitance with increasing active mass, the approach developed in this investigation facilitated the fabrication of anodes, which showed a record-high capacitance of 7 F cm^{-2} in a neutral Na_2SO_4 electrolyte. Of particular importance was a synergy of contributions of CuO and PPy, which resulted in a higher capacitance, lower total resistance, and reduced charge transfer resistance of composite CuO-PPy electrodes compared to the electrodes of the same mass containing only individual components. The synergistic effect of CuO and PPy was linked to the interfacial charge transfer phenomena and beneficial effect of the dopant used for the PPy synthesis. The contribution of interfacial and diffusion components to the total capacitance was analyzed. We successfully addressed the problem of lower capacitance of supercapacitor anodes compared to the capacitance of advanced supercapacitor cathodes. The ability to match the capacitance of advanced Mn_3O_4 cathodes in aqueous electrolytes facilitated the fabrication of asymmetric devices, which showed enhanced capacitive properties and high energy density. The obtained devices are promising for energy storage and capacitive water deionization applications.

EXPERIMENTAL PROCEDURES

Copper chloride dihydrate ($CuCl_2·2H_2O$), NaOH, polyvinyl butyral (PVB), pyrrole (Py), ammonium persulfate (APS), and 4,5-dihydroxy-1,3-benzenedisulfonic acid disodium salt monohydrate (Tiron) were supplied by Aldrich, Canada. Multiwalled carbon nanotubes (MWCNTs, ID 4.8 nm, OD 11.7 nm, length 1 μm) were supplied by Bayer, Germany, and used as conductive additives. Ni foams (thickness 1.7 mm, 95% porosity; Vale, Canada) were used as current collectors.

For the synthesis of the CuO nanomaterial, 40 mmol of NaOH was dissolved in 50 mL of distilled water with stirring. Subsequently, 20 mmol of $CuCl_2·H_2O$ was added to the NaOH solution, resulting in the immediate formation of bluish $Cu(OH)_2$ precipitate. The solution was continuously stirred for 12 h and then transferred into a 100 mL Teflon-lined autoclave. The autoclave was maintained at 100 °C for 16 h. The formed dark precipitate was washed and centrifuged multiple times with DI water and ethanol. Finally, the product was dried at 55 °C for 12 h.

The synthesis of polypyrrole (PPy) was achieved with Py reagent added to DI water at 4 °C. Tiron was added as a dopant for Py with a Py/Tiron molar ratio of 10:1. Then APS was added dropwise as an oxidizing agent to the solution with a Py/APS molar ratio of 1:1. The mixture was stirred for 2 h to complete the chemical polymerization reaction. Subsequently, Tiron-doped PPy was washed with DI water and dried for 24 h.

The electrodes for electrochemical testing contained PPy, CuO, or their composites. The CuO/PPy mass ratio was 80/20, 70/30, 50/50, 40/60, 30/70, and 20/80 in PPy-CuO 80, PPy-CuO 70, PPy-CuO 50, PPy-CuO 40, PPy-CuO 30, and PPy-CuO 20 composites, respectively. The MWCNT content in the composites was 20% of the total mass of PPy and CuO. Ni foams were impregnated with slurries containing PPy, CuO, and MWCNT in ethanol and PVB as a binder. The mass of the PVB was 3% of the total mass of PPy, CuO, and MWCNT. The mass of the impregnated material after drying was 40 mg cm^{-2}. Impregnated foam electrodes with an area of 1 cm^2 were compressed to 37% of their initial thickness to increase the electrical contact between the active material and the Ni foam.

Transmission electron microscopy (TEM) investigations were conducted using a Talos L120C (USA) instrument, and the X-ray diffraction (XRD) spectrum was acquired with a diffractometer (Bruker D8 Advance, Cu Kα radiation, UK). Scanning electron microscopy (SEM) studies were performed using a JEOL 6610LV (Japan) microscope. All electrochemical investigations, including cyclic voltammetry (CV), electrochemical impedance spectroscopy (EIS), and galvanostatic charge−discharge (GCD) studies, were performed using a VMP 300 Biologic potentiostat. All the electrochemical tests of the electrodes were studied in a three-electrode cell using 0.5 M Na_2SO_4 aqueous solutions. A standard calomel electrode (SCE) as a reference electrode and a Pt gauze as a counter electrode were used. EIS studies were performed at a voltage amplitude of 5 mV.

Areal (C_S) and gravimetric (C_m) capacitances were derived from the CV data using the following equation:

$$C = \frac{\Delta Q}{\Delta U} = \frac{\left|\int_0^{t(U_{max})} I dt\right| + \left|\int_{t(U_{max})}^0 I dt\right|}{2U_{max}} \quad (1)$$

where ΔQ is the charge, $I$is the current, and $\Delta U$is the potential range, and from the chronopotentiometry data:

$$C = I\Delta t/\Delta U \quad (2)$$

The complex capacitance $C^*(\omega) = C'(\omega) - iC''(\omega)$ was derived at different frequencies (ω) from the complex impedance $Z^*(\omega) = Z'(\omega) + iZ''(\omega)$:

$$C'(\omega) = \frac{-Z''(\omega)}{\omega|Z(\omega)|^2} \quad (3)$$

$$C''(\omega) = \frac{Z'(\omega)}{\omega|Z(\omega)|^2} \quad (4)$$

The equivalent circuit used for the analysis of EIS data for electrodes with high active mass loading was described in ref 21. The data analysis was performed using a ZFit tool in the EC-lab software.

https://doi.org/10.1021/acsaem.4c01204
ACS Appl. Energy Mater. 2024, 7, 5572−5581

The procedure for the fabrication of Mn_3O_4 cathodes with an active mass of 40 mg cm^{-2} and capacitances of 5.58 and 3.83 F cm^{-2} at 1 and 100 mV s^{-1}, respectively, in 0.5 M Na_2SO_4 electrolyte was described in a previous investigation.[20]

RESULTS AND DISCUSSION

Previous investigations showed that advances in chemical synthesis of nanostructured CuO can result in significant improvement in the capacitive behavior of this material.[7,11] Therefore, hydrothermal synthesis was used for the fabrication of the CuO electrodes. Figure 1 shows the X-ray diffraction

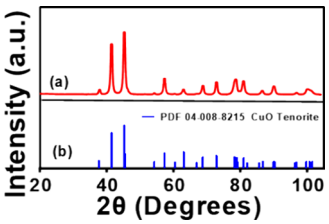

Figure 1. (a) X-ray diffraction pattern of prepared CuO. (b) PDF 04-008-8215 of CuO.

pattern of the prepared CuO powder. The diffraction peaks correspond to JCPDS file 04-008-8215 and indicate the formation of a single-phase CuO material.

TEM data at different magnifications are presented in Figure 2. Figure 2A shows a maple-leaf-like CuO nanoparticle agglomeration with a 100−400 nm size. TEM at higher magnifications showed that the agglomerates contained small particles with a typical size below 20 nm (Figure 2B,C). The small particle size is beneficial for supercapacitor applications because it facilitates the electrolyte access to the particle surface. However, it is important to note that previous investigations of different materials did not show a correlation between electrochemical capacitance and BET surface area.[35−37]

Electrochemical testing was performed in a voltage window of −0.5 to +0.4 V versus SCE. Previous investigations showed that this voltage window is ideal for achieving the highest capacitance of pure PPy electrodes.[38,39] Investigations of CuO-based electrodes and composites also showed good performance in this window.[8,12,14]

SEM studies (Supporting Information, Figures S1 and S2) of CuO and PPy electrodes showed small pores, which were beneficial for electrolyte diffusion. Figure 3 shows the electrochemical testing results for CuO electrodes. The CVs (Figure 3A) deviated significantly from the ideal rectangular shape. The current increased with increasing scan rate. The capacitance for the CuO electrode was 0.11 F cm^{-2} at 1 mV s^{-1} and decreased to 0.057 F cm^{-2} at 100 mV s^{-1} (Figure 3B). Figure 3C shows EIS data in a Nyquist plot, which indicated that the CuO electrode exhibited relatively high resistance $R = Z'$.

The C_S' calculated from the EIS data was 0.045 F cm^{-2} at a frequency of 10 mHz (Figure 3D). The low-frequency C_S' was comparable with that of C_S calculated from the CV data obtained at low scan rates. Frequency dependence of C_S'' showed a maximum at a relatively high frequency, which indicated good capacitance retention. Galvanostatic charge−discharge (GCD) analysis was performed at different charge−discharge rates (Figure 3E). A short discharge time indicated a relatively small capacitance, which was found to be 0.07 F cm^{-2} at 3 mA cm^{-2}, and the capacitance decreased to 0.055 F cm^{-2} at 40 mA cm^{-2} current density (Figure 3F).

The charge storage mechanism of CuO can be attributed to the redox reactions of Cu ions. Surface chemistry plays a critical role in the properties of nanoparticles. The crystalline structure of thin surface layers is different from the structure of the bulk of the nanocrystals. The reduction of crystal size usually results in an increasing number of surface atoms, which interact with ions from solutions. For example, $Mn^{4+}O_2$ particles adsorb Na ions from solutions to form $Na^+_\delta Mn^{3+}_\delta Mn^{4+}_{(1-\delta)}O_2$ on the particle surface, which governs the remarkable pseudocapacitive properties[40] of MnO_2 in the positive potential range, where Mn^{3+} is oxidized to Mn^{4+}. It is suggested that Na ions from Na_2SO_4 solutions are adsorbed on CuO nanoparticles to form $Na^+_\delta Cu^+_\delta Cu^{2+}_{(1-\delta)}O$. It is in this regard that many investigations[41−45] described the formation of solid solutions $Na_xCu_{(1-x)}O_y$ (x = 0.01−0.1) or Na-doped CuO. Na ions can be incorporated in the CuO structure by chemical synthesis or treatment in an electric field.[41−45] Moreover, Na^+ ions can be adsorbed on CuO in Na_2SO_4 solutions. It is hypothesized that the charge storage mechanism of CuO in the Na_2SO_4 electrolyte can be described by the following reactions:

$$Na^+_\delta Cu^+_\delta Cu^{2+}_{(1-\delta)}O + \gamma e^- + \gamma Na^+ \leftrightarrow Na^+_{\delta+\gamma} Cu^+_{\delta+\gamma} Cu^{2+}_{(1-\delta-\gamma)}O \quad (5)$$

in the negative potential range and

$$Na^+_\delta Cu^+_\delta Cu^{2+}_{(1-\delta)}O \leftrightarrow Na^+_{\delta-\alpha} Cu^+_{\delta-\alpha} Cu^{2+}_{(1-\delta+\alpha)}O + \alpha e^- + \alpha Na^+ \quad (6)$$

in the positive potential range. The redox peaks in Figure 3A at 0.35−0.4 V can result from deintercalation/intercalation reactions of Na ions, as it was described in a previous investigation,[46] in agreement with eq 6. Small peaks were also observed in the negative potential range at −0.4 to −0.1 V due to the reduction of Cu^{2+} to Cu^{1+}, as it was described in the

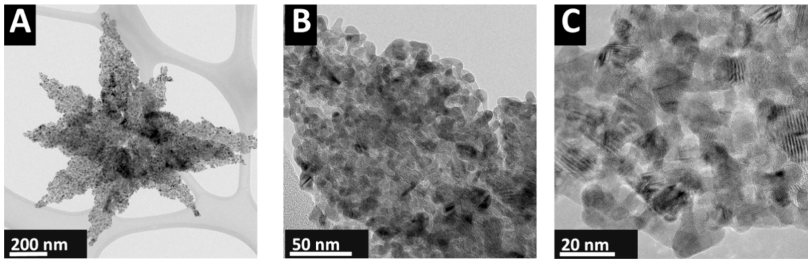

Figure 2. (A−C) TEM images at different magnifications for as-prepared CuO.

https://doi.org/10.1021/acsaem.4c01204
ACS Appl. Energy Mater. 2024, 7, 5572−5581

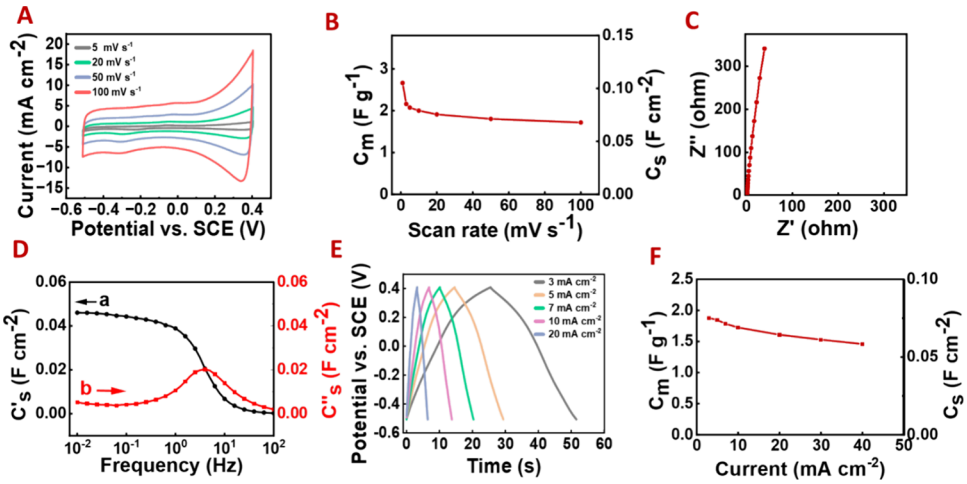

Figure 3. (A) CVs at different scan rates, (B) capacitance versus scan rate, (C) Nyquist EIS plot, (D) components of complex capacitance versus frequency, (E) GCD data at different current densities, and (F) capacitance calculated from GCD data versus current density for CuO electrodes.

literature,[5,47,48] in agreement with eq 5. However, the intensities of such peaks were low because of the high resistance (Figure 3C) of the electrode material.

The investigations of CuO electrodes showed relatively low gravimetric capacitance, which resulted in low areal capacitance. This can be attributed to the poor electrolyte access to the CuO particles in high active mass electrodes and low electronic conductivity of the electrode material. However, a remarkable increase in capacitance was observed in CuO-PPy composites, which showed significantly higher capacitance compared to the capacitances of the individual components. The fabrication of such composites allowed for enhanced utilization of capacitive properties of CuO. The high capacitance of the CuO-PPy composite electrodes resulted from the synergy of contributions of the individual components.

The SEM studies of composite electrodes showed particles of individual components and small pores, which were beneficial for electrolyte diffusion (Figure S3). Figure 4A compares CVs for CuO-PPy and PPy electrodes. The addition of PPy to CuO resulted in a significant increase in currents, especially for low electrode potentials. The redox reactions of CuO and PPy contributed to the observed currents, influencing the CV shapes and capacitive properties of the composites. The CVs for pure PPy electrodes exhibited nearly rectangular shapes without redox peaks. This can be attributed to the fast reversible redox reactions of PPy as described in the literature.[49] The CVs of the composites showed small broad redox peaks in the range of −0.15 to −0.3 V. The peaks can be attributed to redox Cu^{2+}/Cu^{1+} reactions.[5,47,48] It is suggested that conductive PPy can facilitate charge transfer and influence the rate of such reactions. The slight shift of electrode potentials of the peaks with changing electrode composition can result from different factors, such as CuO content in the composites, electrode bulk microstructure and electrical conductivity, charge transfer, and ion diffusion kinetics, which were also dependent on PPy and CuO content in the high active mass electrodes. The capacitances at 1 mV s^{-1} for composites containing 20−40% CuO were higher than the capacitance of electrodes containing individual PPy or CuO materials (Figure 4B and Table1). Moreover, the composite materials showed an enhanced capacitance retention at high scan rates. The highest capacitance of 7 F cm^{-2} at 1 mV s^{-1} was obtained for PPy-CuO 20 composite. The PPy-CuO 30 composite showed a capacitance of 6.9 F cm^{-2} at a current of 1 mV s^{-1}. However, the PPy-CuO 30 composite showed better capacitance retention at high scan rates and showed a capacitance of 3.6 F cm^{-2} at 100 mV s^{-1}.

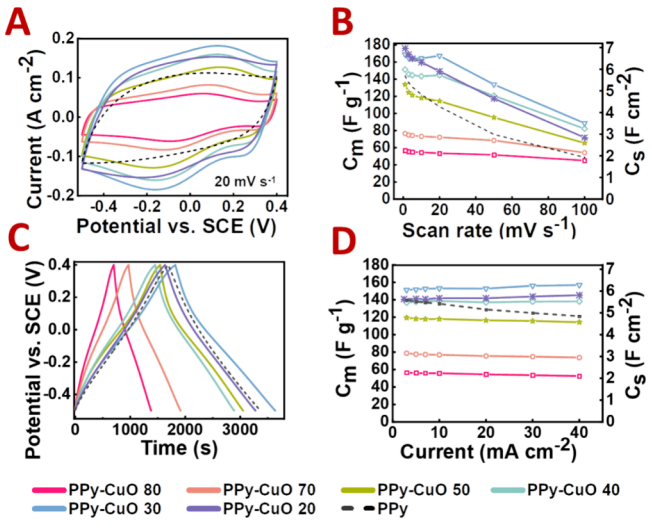

Figure 4. (A) CVs at 20 mV s^{-1}, (B) capacitance obtained from CV data versus scan rate, (C) GCD data at 3 mA cm^{-2}, and (D) capacitances obtained from GCD data versus current density for different electrodes.

GCD data showed nearly triangular charge−discharge curves (Figure 4C). Moreover, the GCD data confirmed the superior behavior of the PPy-CuO 30 composite compared to other composites and PPy (Figure 4D and Table 1). The capacitance of the PPy-CuO 30 composite is higher than the capacitance of other anode materials of the same mass.[1] As pointed out above, the lower capacitance of anode materials compared to the capacitance of cathode materials is a limiting factor for the fabrication of asymmetric supercapacitor devices. However, the capacitance of the PPy-CuO-30 composite is on par with capacitances of advanced cathode materials[1] such as MnO_2 and Mn_3O_4. It is suggested that the enhanced capacitance of the composites resulted from the synergy of contributions of the individual components. This is especially evident from the

https://doi.org/10.1021/acsaem.4c01204
ACS Appl. Energy Mater. 2024, 7, 5572−5581

Table 1. Capacitances Obtained from CV and GCD Data

	capacitance from CV data				capacitance from GCD data			
	1 mV s^{-1}		100 mV s^{-1}		3 mA cm^{-2}		40 mA cm^{-2}	
electrode	C_S, F cm^{-2}	C_m, F g^{-1}	C_S, F cm^{-2}	C_m, F g^{-1}	C_S, F cm^{-2}	C_m, F g^{-1}	C_S, F cm^{-2}	C_m, F g^{-1}
CuO	0.1	2.6	0.068	1.7	0.07	1.9	0.058	1.46
PPy-CuO 80	2.3	56.7	1.8	45	2.2	56.4	2.1	52.6
PPy-CuO 70	3.0	76.57	2.1	54.2	3.1	77.4	2.9	72.5
PPy-CuO 50	5.4	133.9	2.6	65.4	4.7	119.4	4.5	114.2
PPy-CuO 40	6.0	151.2	3.2	82	5.4	127.1	5.5	140
PPy-CuO 30	6.9	168.8	3.6	133.8	6	149.1	6.2	154.6
PPy-CuO 20	7.0	176	2.8	117.4	5.6	141.1	5.8	146.7
PPy	5.7	143	1.9	48.7	5.5	140.7	5.6	122.2

experimental data presented in Figure 5. The dependences of capacitance versus composition at different scan rates show

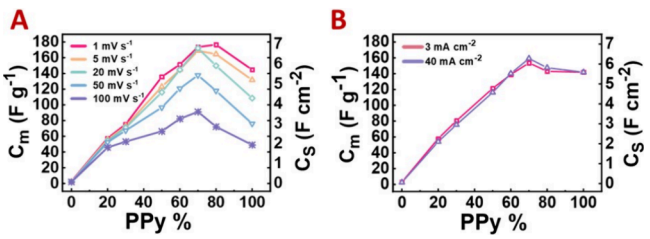

Figure 5. Capacitances (A) obtained at different scan rates from CV data and (B) obtained at different current densities from GCD data versus the composition of the electrodes.

maxima. It is seen that significantly higher capacitances can be achieved in the composite materials compared to the capacitances of CuO or PPy. A linear approximation based on the independent contributions of the individual components gives significantly lower capacitance compared to the experimental data:

$$C_C = C_{m1} \times m_1 + C_{m2} \times m_2 \quad (7)$$

where C_C is the capacitance of a composite; C_{m1} and m_1 are gravimetric capacitance and mass of the CuO component, respectively; and C_{m2} and m_2 are gravimetric capacitance and mass of the PPy component, respectively.

The EIS data provided additional evidence of the synergistic effect of CuO and PPy. Composite electrodes showed lower real and imaginary parts of complex impedance compared to CuO (Figure 6A,C). The composites containing 20−40% CuO showed lower real and imaginary parts of impedance compared to PPy. The lower real part of impedance indicated lower resistance, whereas the lower imaginary part indicated higher capacitance. Indeed, the calculations of the real component of capacitance from the impedance data showed that the composites containing 20−40% CuO showed higher capacitance at 10 mHz compared to PPy (Figure 6B). Moreover, such composites showed higher relaxation frequencies corresponding to maxima in the imaginary parts of the imaginary components of the complex capacitance (Figure 6C), which indicated better capacitance retention with increasing frequency. The highest real part of capacitance at 10 mHz was 5.5 F cm^{-2} for the PPy-CuO 30 electrode, in agreement with CV and GCD data. The analysis of the impedance data using an equivalent circuit developed for high active mass electrodes[21] showed that charge transfer resistance has a minimum (0.088 Ω) for PPy-CuO 30 (Figure 6D),

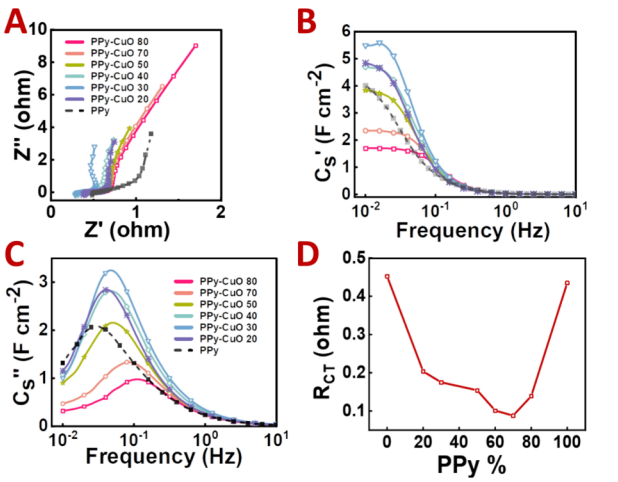

Figure 6. (A) Nyquist plot of EIS data, (B) real component of capacitance (C_S') versus frequency, (C) imaginary component of capacitance (C_S'') versus frequency, and (D) charge transfer resistance of the composites.

which correlated with the high capacitance of this composite. The low total electrode resistance and charge transfer resistance allowed better utilization of the capacitive properties of the electrode materials.

The synergistic effect, which resulted in enhanced properties of composites, is not well understood. The significant difference in the electrical conductivity and dielectric constant of PPy and CuO can promote charge accumulation at their interface due to the Maxwell−Wagner effect and reduction of the potential barrier for charge transfer. This can facilitate charge transfer, which leads to reduced impedance and higher capacitance. It should be noted that nonelectrochemical studies also reported that CuO-PPy composites showed lower electrical resistance than the resistances of the individual components.[50] Interesting and enhanced properties were also observed in other composites containing conductive polymers and metal oxides. Observed phenomena were related to enhanced electron transfer at the PPy-metal oxide interface, which resulted in increased capacitance, magnetoresistance, magnetization, and other properties. For example, the investigations of polyaniline-coated ferromagnetic particles revealed enhanced magnetoresistance,[51] which resulted from spin-polarized electron tunneling facilitated by the conducting polymer. In another investigation, the surface modification of ferromagnetic particles with PPy resulted in a significant increase in magnetization[52] that was higher than theoretically expected. The pseudocapacitance of PPy composites contain-

https://doi.org/10.1021/acsaem.4c01204
ACS Appl. Energy Mater. 2024, 7, 5572−5581

ing ferromagnetic nanoparticles was higher than the capacitance of pure PPy electrodes.[53] Therefore, the investigation of interfacial phenomena and charge transfer at the interface of conductive polymers/metal oxide nanoparticles opens an avenue for the development of advanced supercapacitors and other functional devices. It is also hypothesized that the use of Tiron as a dopant for PPy can contribute to an enhanced charge transfer. Tiron is a catecholate type molecule, which can create strong catecholate bonds to the metal atoms on the surface of metal oxide particles.[54] It was demonstrated that such bonding can result in the formation of a charge transfer complex and enhanced charge transfer.[55]

The analysis of the charge storage mechanism of the electrode materials was performed using CV data and the following equation:[56]

$$i = a\nu^b \tag{8}$$

where i is the measured current, ν is the sweep rate, and a and b are parameters, with the b values derived from the slope of log i vs log ν. It is well-known that parameter b varies from 0.5 to 1. For the battery-type dominating charging mechanism, $0.5 < b < 0.8$, whereas for the dominating pseudocapacitive mechanism, $0.8 < b < 1$, and parameter b equals 1 for the pure capacitive process.[57−61]

Figure 7 shows the dependence of calculated parameter b on the PPy content. For the pure CuO electrode, $b = 0.67$, and the

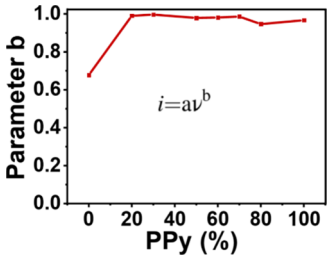

Figure 7. Parameter b vs electrode composition.

battery charging mechanism is dominant. It can be explained by the slow diffusion kinetics due to the high agglomeration as seen in TEM analysis in Figure 2, in agreement with the literature.[60] By adding PPy to CuO, the parameter b values ranged from 0.94 to 0.99 where the pseudocapacitive charging mechanism is dominant. This change in the charging mechanism was due to the enhanced charge transfer, which facilitated redox reactions, and the fast redox reaction led to the pseudocapacitive behavior.

The PPy-CuO 30 composite showed a promising capacitive behavior, and this material was selected for further analysis and application in asymmetric supercapacitor devices. The analysis of capacitive behavior of this electrode was performed using the following equations:[62]

$$i(V) = i_{cap} + i_{diff} = k_1\nu + k_2\nu^{1/2} \tag{9}$$

$$\frac{i(V)}{\nu^{1/2}} = k_1\nu^{1/2} + k_2 \tag{10}$$

where current (i) is a function of potential (V) and can be differentiated into capacitive current (i_{cap}) and current from diffusion-controlled process (i_{diff}). By using eq 10 to plot $i(V)/\nu^{1/2}$ versus $\nu^{1/2}$, slope (k_1) and intercept (k_2) can be evaluated. Differentiated currents are plotted in Figure 8A at different scan rates. A dominant diffusion process at the low scan rate of 1 mV s^{-1} can be noticed due to the dominant Faradaic intercalation process and facilitated electrolyte ion diffusion through the bulk electrode. The diffusion-controlled process was reported to be dependent on the sweep rate, exhibiting a gradual increase in the capacitive process at the electrode surface.[63] The differentiated currents of the PPy-CuO 30 electrode were plotted for a scan rate of 3 mV s^{-1} versus potential in Figure 8B. The sum of diffusion and capacitive controlled contributions (Figure 8B) at all potentials coincides with the experimental CV graph for the PPy-CuO 30 electrode presented in Figure 8C. The contribution of the diffusion current (44% of the total current) is higher than literature data for other materials at the same scan rates.[60,63] The investigation of the cyclic stability of the PPy-CuO 30 electrodes showed (Figure 9) a capacitance retention of

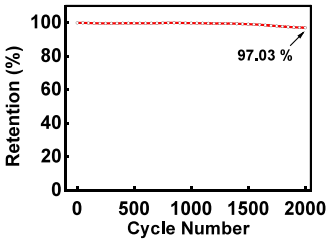

Figure 9. Capacitance retention for PPy-CuO-30 electrodes.

97.03% after 2000 cycles. SEM studies of the electrodes before and after cycling showed electrode stability (Figure S4). It should be noted that other anode materials for asymmetric supercapacitors, such as FeOOH,[64] showed poor cyclic stability. Therefore, PPy-CuO 30 is promising for applications in anodes of supercapacitor devices. The higher capacitance of PPY-CuO 30 compared to other composites can result from a lower charge transfer resistance, which facilitates Faradaic

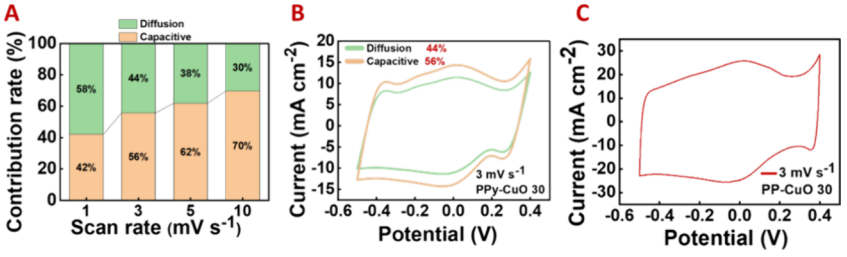

Figure 8. (A) The diffusion and capacitive-controlled contributions to the total charge storage process of the PPy-CuO 30 composite at different CV scan rates at a fixed potential 0.1 V, (B) CV curves of PPy-CuO-30 electrodes recorded at 3 mV s^{-1} divided into diffusion and surface current contributions, and (C) experimental CV for PPy-CuO-30 electrodes recorded at 3 mV s^{-1}.

https://doi.org/10.1021/acsaem.4c01204
ACS Appl. Energy Mater. 2024, 7, 5572−5581

reactions. Such anodes must be combined with advanced cathodes, which exhibit a comparable areal capacitance with a similar active mass loading in the same electrolyte in partially overlapping[65] voltage windows.

Mn_3O_4 and MnO_2 exhibit high capacitance in a voltage window of 0 to +1.0 V versus SCE in Na_2SO_4 electrolyte. The capacitance of 6−8 F cm^{-2} was achieved[1] for MnO_2 electrodes with an active mass of 40 mg cm^{-2}. However, the high resistivity of MnO_2 resulted in significant capacitance reduction with increasing scan rate and in poor capacitance retention at high scan rates.[21] In contrast, Mn_3O_4 electrodes showed good capacitance retention at high scan rates.[20] Mn_3O_4 electrodes with an active mass of 40 mg cm^{-2} showed capacitances of 5.58 and 3.83 F cm^{-2} at scan rates of 1 and 100 mV s^{-1}, respectively.[20] The capacitance of such electrodes was lower at 1 mV s^{-1} and higher at 100 mV s^{-1} than the capacitance of PPy-CuO 30 at the same scan rates. Therefore, Mn_3O_4 electrodes[20] were used because such electrodes allowed for better matching of PPy-CuO-30 capacitance in scan rate range of 1−100 mV s^{-1}. Figure 10 shows the CVs for PPy-CuO 30 and Mn_3O_4 electrodes at 20 mV s^{-1}. The CVs showed comparable areas, which indicated comparable capacitances.

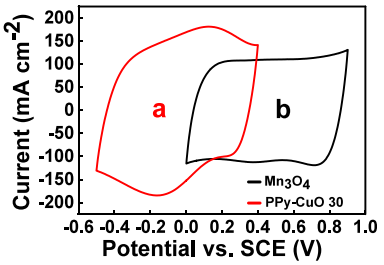

Figure 10. CVs for (a) PPy-CuO 30 and (b) Mn_3O_4 electrodes with an active mass of 40 mg cm^{-2} in the Na_2SO_4 electrolyte.

The asymmetric device was tested in a voltage window of 1.5 V in a 0.5 M Na_2SO_4 electrolyte. The CVs at low scan rates were of nearly ideal rectangular shape (Figure 11A). A capacitance of 2.76 F cm^{-2} was obtained at a scan rate of 1 mV s^{-1}. The device showed a capacitance retention of 33% in the range of 1−100 mV s^{-1} (Figure 11B) and a relatively low impedance (Figure 11C). The relaxation frequency for the complex capacitance was found to be 20 mHz (Figure 11D). Nearly ideal linear charge−discharge dependences were obtained at different current densities (Figure 11E). The capacitance calculated from the GCD data decreased from 2.74 to 2.12 F cm^{-2} with an increasing current density from 3 to 40 mA cm^{-2} (Figure 11F).

The asymmetric devices showed a high energy density of 10.83 Wh kg^{-1} and power density of 373 W kg^{-1} at a current density of 40 mA cm^{-2} (calculated for total mass of 80 mg of both electrodes) and good cyclic stability of 92.02% after 2000 cycles (Figure 12).

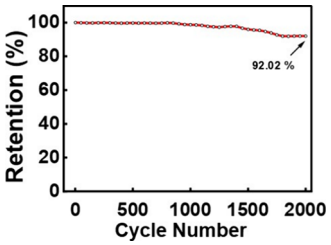

Figure 12. Capacitance retention for the asymmetric device containing PPy-CuO-30 and Mn3O4 electrodes.

CONCLUSIONS

CuO and PPy-CuO electrodes for supercapacitors were fabricated using CuO nanoparticles prepared by hydrothermal synthesis and PPy polymer synthesized by chemical polymerization using Tiron as a dopant. The voltage window was optimized in the range of −0.5 to +0.4 V for the Na_2SO_4 electrolyte, and charge storage mechanisms of CuO were suggested. The synergistic effect of CuO and PPy resulted in the enhanced capacitance of the composite electrodes, reduced impedance, and reduced charge transfer resistance. The enhanced charge transfer properties were linked to the Maxwell−Wagner effect at the materials' interface and

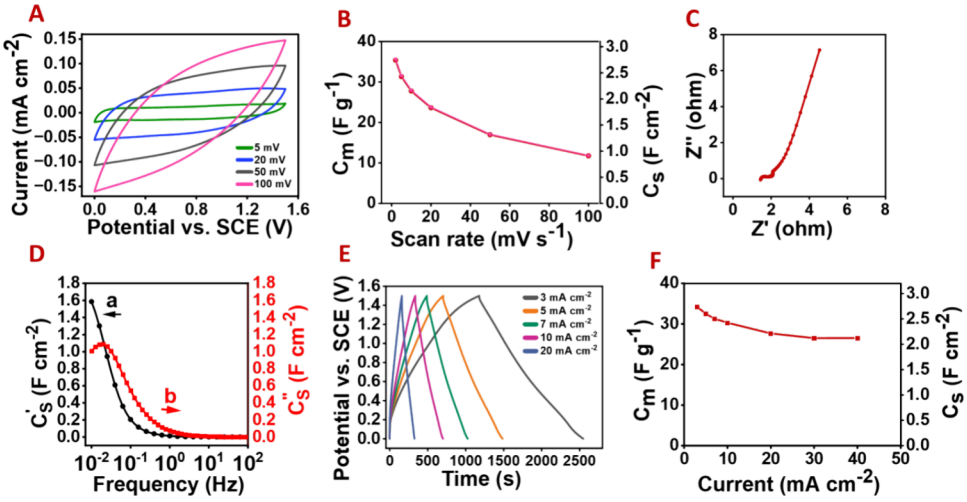

Figure 11. (A) CVs, (B) capacitance as a function of scan rate, (C) EIS impedance data, (D) components of complex capacitance versus frequency, (E) GCD data, and (F) capacitance calculated from GCD data as a function of current density for an asymmetric device containing PPy-CuO 30 anodes and Mn_3O_4 cathodes. The gravimetric capacitance C_m was obtained by normalizing the device capacitance by a total mass of 80 mg of both electrodes.

https://doi.org/10.1021/acsaem.4c01204
ACS Appl. Energy Mater. 2024, 7, 5572−5581

chelating properties of Tiron. A remarkably high capacitance of 7 F cm^{-2} was obtained for the composite electrodes, which exhibited good cyclic stability. This finding eliminates the problems of lower capacitance of negative electrodes compared to the capacitance of advanced positive electrodes and poor cyclic stability of negative electrodes. The obtained results opened an avenue for improved matching of areal capacitances of cathodes and anodes and fabrication of advanced asymmetric supercapacitors. The fabricated asymmetric devices showed a remarkably high capacitance of 2.76 F cm^{-2} in a voltage window of 1.5 V, high energy density of 10.83 Wh kg^{-1} for the device with a total electrode mass of 80 mg cm^{-2}, and excellent cyclic stability. The results obtained stress the importance of interfacial phenomena at the polypyrrole−metal oxide interface that can potentially be used for other energy storage devices.

■ ASSOCIATED CONTENT

Supporting Information

The Supporting Information is available free of charge at https://pubs.acs.org/doi/10.1021/acsaem.4c01204.

SEM image of the CuO electrode (Figure S1); SEM image of the PPy electrode (Figure S2); SEM image of the PPy-CuO 30 electrode (Figure S3); and SEM image of the PPy-CuO 30 electrode (A) before and (B) after cycling (Figure S4) (PDF)

■ AUTHOR INFORMATION

Corresponding Author

Igor Zhitomirsky − *Department of Materials Science and Engineering, McMaster University, Hamilton, Ontario L8S 4L8, Canada;* orcid.org/0000-0002-0435-1591; Email: zhitom@mcmaster.ca

Authors

Mahmoud Awad − *Department of Materials Science and Engineering, McMaster University, Hamilton, Ontario L8S 4L8, Canada*

Mohamed Nawwar − *Technical Research Center (TRC), Cairo 11759, Egypt*

Complete contact information is available at: https://pubs.acs.org/10.1021/acsaem.4c01204

Notes

The authors declare no competing financial interest.

■ ACKNOWLEDGMENTS

Research supported by the Natural Sciences and Engineering Research Council of Canada, grant RGPIN-2018-04014, and CRC program. Electron microscopy studies were performed at the Canadian Centre for Electron Microscopy.

■ REFERENCES

(1) Chen, R.; Yu, M.; Sahu, R. P.; Puri, I. K.; Zhitomirsky, I. The Development of Pseudocapacitor Electrodes and Devices with High Active Mass Loading. *Adv. Energy Mater.* **2020**, *10* (20), 1903848.

(2) Sharma, P.; Parashar, P.; Ghosh, D.; Yadav, D.; Rawat, P.; Majumder, S. A Review on Microwave Assisted Synthesis of Transition Metal Oxides and their Potent Application as Supercapacitors. *ChemistrySelect* **2023**, *8* (47), No. e202303467.

(3) Wu, Y.; Li, S.; Ning, F.; Wang, G.; Wang, T.; Chen, T. Multi-Dimensional Binary Micro CuCo2O4/Nano NiCo2S4 for High-Performance Supercapacitors. *ChemistrySelect* **2023**, *8* (43), No. e202303003.

(4) Chavan, R.; Kamble, G.; Kashale, A.; Kolekar, S.; Sathe, B.; Ghule, A. Facile, Cost Effective and Eco-friendly Approach to Synthesize Bio-MnO2 Nanosphered Thin Filmfor all Solid-State Flexible Asymmetric Supercapacitor. *ChemistrySelect* **2022**, *7* (33), No. e202202166.

(5) Wang, D.; Haque, S.; Williams, T.; Karim, F.; Hariharalakshmanan, R. K.; Al-Mayalee, K. H.; Karabacak, T. Cyclic voltammetry and specific capacitance studies of copper oxide nanostructures grown by hot water treatment. *MRS Adv.* **2023**, 1−7.

(6) Wang, Q.; Wang, Y. Re-Examination of CuO Reduction Steps and Understanding of the Factors Influencing the Cyclic Voltammetry Profile of CuO. *J. Electrochem. Soc.* **2018**, *165* (11), A2439.

(7) Zhang, H.; Zhang, M. Synthesis of CuO nanocrystalline and their application as electrode materials for capacitors. *Mater. Chem. Phys.* **2008**, *108* (2−3), 184−187.

(8) Asl, H. Z.; Rozati, S. M. Influence of structural properties on the electrochemical performance of FTO/CuO double-layer thin-film spray-deposited from different precursor solutions. *Appl. Phys. A: Mater. Sci. Process.* **2023**, *129* (11), 786.

(9) Bilgin, S.; Alver, Ü.; Erdemir, F.; Çanakçı, A. Effect of fuel type on pseudocapacitance behaviour of CuO nanoparticles synthesized by solution combustion method. *Bull. Mater. Sci.* **2022**, *45* (4), 240.

(10) Liu, Y.; Cao, X.; Jiang, D.; Jia, D.; Liu, J. Hierarchical CuO nanorod arrays in situ generated on three-dimensional copper foam via cyclic voltammetry oxidation for high-performance supercapacitors. *Journal of Materials Chemistry A* **2018**, *6* (22), 10474−10483.

(11) Wang, G.; Huang, J.; Chen, S.; Gao, Y.; Cao, D. Preparation and supercapacitance of CuO nanosheet arrays grown on nickel foam. *J. Power Sources* **2011**, *196* (13), 5756−5760.

(12) Dubal, D. P.; Gund, G. S.; Lokhande, C. D.; Holze, R. CuO cauliflowers for supercapacitor application: Novel potentiodynamic deposition. *Mater. Res. Bull.* **2013**, *48* (2), 923−928.

(13) Indumathi, N.; Sridevi, C.; Gowdhaman, A.; Ramesh, R. Synthesis, structural analysis, and electrochemical performance of chitosan incorporated CuO nanomaterial for supercapacitor applications. *Inorg. Chem. Commun.* **2023**, *156*, No. 111222.

(14) Huang, J.; Zheng, X.; Xing, Z.; Tian, L. Controllable Fabrication of CuO Nanostructures on Nickel Foam by Electrodeposition Method for High-Performance Supercapacitors. *Nano* **2022**, *17* (13), 2250098.

(15) Bhise, S. C.; Awale, D. V.; Vadiyar, M. M.; Patil, S. K.; Kokare, B. N.; Kolekar, S. S. Facile synthesis of CuO nanosheets as electrode for supercapacitor with long cyclic stability in novel methyl imidazole-based ionic liquid electrolyte. *J. Solid State Electrochem.* **2017**, *21*, 2585−2591.

(16) Sudhakar, Y.; Hemant, H.; Nitinkumar, S.; Poornesh, P.; Selvakumar, M. Green synthesis and electrochemical characterization of rGO−CuO nanocomposites for supercapacitor applications. *Ionics* **2017**, *23*, 1267−1276.

(17) Arun, L.; Karthikeyan, C.; Philip, D.; Sasikumar, M.; Elanthamilan, E.; Merlin, J. P.; Unni, C. Effect of Ni 2+ doping on chemocatalytic and supercapacitor performance of biosynthesized nanostructured CuO. *Journal of Materials Science: Materials in Electronics* **2018**, *29*, 21180−21193.

(18) Chaudhary, M.; Singh, M.; Kumar, A.; Prachi; Gautam, Y. K.; Malik, A. K.; Kumar, Y.; Singh, B. P. Experimental investigation of Co and Fe-Doped CuO nanostructured electrode material for remarkable electrochemical performance. *Ceram. Int.* **2021**, *47* (2), 2094−2106.

(19) Zhang, J.; Huang, R.; Dong, Z.; Lin, H.; Han, S. An illumination-assisted supercapacitor of rice-like CuO nanosheet coated flexible carbon fiber. *Electrochim. Acta* **2022**, *430*, No. 140789.

(20) Awad, M.; Zhitomirsky, I. Boosting the activation rate and capacitance retention of MnOx electrodes prepared using capping agents. *Colloids Surf., A* **2023**, *676*, No. 132176.

(21) Wang, Y.; Liu, Y.; Zhitomirsky, I. Surface modification of MnO 2 and carbon nanotubes using organic dyes for nanotechnology of

electrochemical supercapacitors. *Journal of Materials Chemistry A* **2013**, *1* (40), 12519−12526.
(22) Krishna Paul, T.; Parvez, M. S.; Mashfik Ahmed, C. Recent Progress and Prospects of MXene/Cellulose-Based Composite Electrodes: A Sustainable Pathway towards Supercapacitor Application. *ChemElectroChem.* **2024**, *11* (2), No. e202300435.
(23) Gowrisankar, A.; Selvaraju, T. α-MnO2-Sensitized SrCO3−Sr(OH)2 Supported on Two-Dimensional Carbon Composites as Stable Electrode Material for Asymmetric Supercapacitor and Oxygen Evolution Catalysis. *ChemElectroChem.* **2022**, *9* (10), No. e202200213.
(24) Brousse, T.; Toupin, M.; Belanger, D. A hybrid activated carbon-manganese dioxide capacitor using a mild aqueous electrolyte. *J. Electrochem. Soc.* **2004**, *151* (4), A614.
(25) Brousse, T.; Bélanger, D. A hybrid Fe3O4-MnO2 capacitor in mild aqueous electrolyte. *Electrochem. Solid-State Lett.* **2003**, *6* (11), A244.
(26) Helli, M.; Sadrnezhaad, S.; Hosseini-Hosseinabad, S.; Vahdatkhah, P. Synthesis and characterization of CuO microflowers/PPy nanowires nanocomposites as high-capacity anode material for lithium-ion batteries. *J. Appl. Electrochem.* **2024**, *54*, 1−11.
(27) Yin, Z.; Ding, Y.; Zheng, Q.; Guan, L. CuO/polypyrrole core−shell nanocomposites as anode materials for lithium-ion batteries. *Electrochemistry communications* **2012**, *20*, 40−43.
(28) Zhou, Y.; Jin, X.; Ni, J.; Zhang, S.; Yang, J.; Liu, P.; Wang, Z.; Lei, J. Evaporation induced uniform polypyrrole coating on CuO arrays for free-standing high lithium storage anode. *J. Solid State Electrochem.* **2019**, *23*, 1829−1836.
(29) Yin, Z.; Fan, W.; Ding, Y.; Li, J.; Guan, L.; Zheng, Q. Shell structure control of PPy-modified CuO composite nanoleaves for lithium batteries with improved cyclic performance. *ACS Sustainable Chem. Eng.* **2015**, *3* (3), 507−517.
(30) Shen, M.; Chen, L.; Ren, S.; Chen, Y.; Li, W.; Zheng, R.; Lin, Y.; Han, D. Construction of CuO/PPy heterojunction nanowire arrays on copper foam as integrated binder-free electrode material for high-performance supercapacitor. *J. Electroanal. Chem.* **2021**, *891*, No. 115272.
(31) Tang, D.; Zhitomirsky, I. Pseudocapacitive properties of polypyrrole−ferrimagnetic CoFe2O4 composites. *Electrochim. Acta* **2024**, *475*, No. 143671.
(32) Qian, T.; Zhou, J.; Xu, N.; Yang, T.; Shen, X.; Liu, X.; Wu, S.; Yan, C. On-chip supercapacitors with ultrahigh volumetric performance based on electrochemically co-deposited CuO/polypyrrole nanosheet arrays. *Nanotechnology* **2015**, *26* (42), No. 425402.
(33) Ates, M.; Serin, M. A.; Ekmen, I.; Ertas, Y. N. Supercapacitor behaviors of polyaniline/CuO, polypyrrole/CuO and PEDOT/CuO nanocomposites. *Polym. Bull.* **2015**, *72*, 2573−2589.
(34) Xu, J.; Wang, D.; Yuan, Y.; Wei, W.; Gu, S.; Liu, R.; Wang, X.; Liu, L.; Xu, W. Polypyrrole-coated cotton fabrics for flexible supercapacitor electrodes prepared using CuO nanoparticles as template. *Cellulose* **2015**, *22*, 1355−1363.
(35) Reddy, R. N.; Reddy, R. G. Sol−gel MnO2 as an electrode material for electrochemical capacitors. *J. Power Sources* **2003**, *124* (1), 330−337.
(36) Jeong, Y.; Manthiram, A. Nanocrystalline manganese oxides for electrochemical capacitors with neutral electrolytes. *J. Electrochem. Soc.* **2002**, *149* (11), A1419.
(37) Dong, W.; Sakamoto, J. S.; Dunn, B. Electrochemical properties of vanadium oxide aerogels. *Sci. Technol. Adv. Mater.* **2003**, *4* (1), 3−11.
(38) Ariyanayagamkumarappa, D.; Zhitomirsky, I. Electropolymerization of polypyrrole films on stainless steel substrates for electrodes of electrochemical supercapacitors. *Synth. Met.* **2012**, *162* (9−10), 868−872.
(39) Shi, C.; Zhitomirsky, I. Electrodeposition and Capacitive Behavior of Films for Electrodes of Electrochemical Supercapacitors. *Nanoscale Res. Lett.* **2010**, *5* (3), 518.
(40) Wei, W.; Cui, X.; Chen, W.; Ivey, D. G. Manganese oxide-based materials as electrochemical supercapacitor electrodes. *Chem. Soc. Rev.* **2011**, *40* (3), 1697−1721.
(41) Sahin, B.; Kaya, T. Highly improved hydration level sensing properties of copper oxide films with sodium and potassium doping. *Appl. Surf. Sci.* **2016**, *362*, 532−537.
(42) Rao, B. N.; Rao, P. T.; Basha, S. E.; Prasanna, D. S. L.; Samatha, K.; Ramachandra, R. K. Exploring the optical and biological aspects of sodium-doped CuO nanoparticles. *Mater. Chem. Phys.* **2023**, *308*, No. 128174.
(43) Siddiqui, H.; Parra, M. R.; Qureshi, M.; Malik, M.; Haque, F. Z. Studies of structural, optical, and electrical properties associated with defects in sodium-doped copper oxide (CuO/Na) nanostructures. *J. Mater. Sci.* **2018**, *53* (12), 8826−8843.
(44) Hu, S.; Liu, H.; Zheng, H.; Jia, S.; Chen, G.; Jiang, R.; Li, L.; Zhao, L.; Zhao, D.; Wang, J. Coating-mediated nanomechanical behaviors of CuO electrodes in Li-and Na-ion batteries. *Adv. Mater. Interfaces* **2020**, *7* (21), 2001161.
(45) Bathwar, M. Na doped CuO as a new day-Night (Photo) catalyst. *J. Nanopart. Res.* **2023**, *25* (7), 142.
(46) Janene, F.; Dhaouadi, H.; Arfaoui, L.; Etteyeb, N.; Touati, F. Nanoplate-like CuO: hydrothermal synthesis, characterization, and electrochemical properties. *Ionics* **2016**, *22*, 1395−1403.
(47) Heng, B.; Qing, C.; Sun, D.; Wang, B.; Wang, H.; Tang, Y. Rapid synthesis of CuO nanoribbons and nanoflowers from the same reaction system, and a comparison of their supercapacitor performance. *RSC Adv.* **2013**, *3* (36), 15719−15726.
(48) Krishnamoorthy, K.; Kim, S.-J. Growth, characterization and electrochemical properties of hierarchical CuO nanostructures for supercapacitor applications. *Mater. Res. Bull.* **2013**, *48* (9), 3136−3139.
(49) Snook, G. A.; Kao, P.; Best, A. S. Conducting-polymer-based supercapacitor devices and electrodes. *J. Power Sources* **2011**, *196* (1), 1−12.
(50) Malook, K.; Ihsan-ul-Haque; Khan, M.; Ali, M. Polypyrrole-CuO based composites, promotional effects of CuO contents on polypyrrole characteristics. *J. Mater. Sci.: Mater. Electron.* **2019**, *30*, 3882−3888.
(51) Gupta, K.; Jana, P. C.; Meikap, A. K.; Nath, T. K. Synthesis of La0. 67Sr0. 33MnO3 and polyaniline nanocomposite with its electrical and magneto-transport properties. *J. Appl. Phys.* **2010**, *107* (7), No. 073704.
(52) Pana, O.; Soran, M. L.; Leostean, C.; Macavei, S.; Gautron, E.; Teodorescu, C. M.; Gheorghe, N.; Chauvet, O. Interface charge transfer in polypyrrole coated perovskite Manganite magnetic nanoparticles. *J. Appl. Phys.* **2012**, *111* (4), No. 044309.
(53) Amarnath, C. A.; Ghamouss, F.; Schmaltz, B.; Autret-Lambert, C.; Roger, S.; Gervais, F.; Tran-Van, F. Polypyrrole/lanthanum strontium Manganite oxide nanocomposites: Elaboration and characterization. *Synthetic metals* **2013**, *167*, 18−24.
(54) Ata, M.; Liu, Y.; Zhitomirsky, I. A review of new methods of surface chemical modification, dispersion and electrophoretic deposition of metal oxide particles. *Rsc Advances* **2014**, *4* (43), 22716−22732.
(55) Wang, G.-L.; Xu, J.-J.; Chen, H.-Y. Dopamine sensitized nanoporous TiO2 film on electrodes: photoelectrochemical sensing of NADH under visible irradiation. *Biosens. Bioelectron.* **2009**, *24* (8), 2494−2498.
(56) Girard, H.-L.; Wang, H.; D'Entremont, A. L.; Pilon, L. Enhancing Faradaic Charge Storage Contribution in Hybrid Pseudocapacitors. *Electrochim. Acta* **2015**, *182*, 639−651.
(57) Chodankar, N. R.; Rama Raju, G. S.; Park, B.; Shinde, P. A.; Chan Jun, S.; Dubal, D. P.; Huh, Y. S.; Han, Y.-K. Potentiodynamic polarization assisted phosphorus-containing amorphous trimetal hydroxide nanofibers for highly efficient hybrid supercapacitors. *Journal of Materials Chemistry A* **2020**, *8* (11), 5721−5733.
(58) Chodankar, N. R.; Shinde, P. A.; Patil, S. J.; Hwang, S.-K.; Raju, G. S. R.; Ranjith, K. S.; Dubal, D. P.; Huh, Y. S.; Han, Y.-K. Solution-free self-assembled growth of ordered tricopper phosphide for

https://doi.org/10.1021/acsaem.4c01204
ACS Appl. Energy Mater. 2024, 7, 5572−5581

efficient and stable hybrid supercapacitor. *Energy Storage Materials* **2021**, *39*, 194−202.
(59) Patil, S. J.; Chodankar, N. R.; Hwang, S.-K.; Raju, G. S. R.; Ranjith, K. S.; Huh, Y. S.; Han, Y.-K. Ultra-stable flexible Zn-ion capacitor with pseudocapacitive 2D layered niobium oxyphosphides. *Energy Storage Materials* **2022**, *45*, 1040−1051.
(60) Okhay, O.; Tkach, A. Graphene/Reduced Graphene Oxide-Carbon Nanotubes Composite Electrodes: From Capacitive to Battery-Type Behaviour. *Nanomaterials* **2021**, *11* (5), 1240.
(61) Gogotsi, Y.; Penner, R. M. Energy Storage in Nanomaterials − Capacitive, Pseudocapacitive, or Battery-like? *ACS Nano* **2018**, *12* (3), 2081−2083.
(62) Liu, J.; Wang, J.; Xu, C.; Jiang, H.; Li, C.; Zhang, L.; Lin, J.; Shen, Z. X. Advanced Energy Storage Devices: Basic Principles, Analytical Methods, and Rational Materials Design. *Adv. Sci.* **2018**, *5* (1), 1700322.
(63) Yan, W.; Kim, J. Y.; Xing, W.; Donavan, K. C.; Ayvazian, T.; Penner, R. M. Lithographically Patterned Gold/Manganese Dioxide Core/Shell Nanowires for High Capacity, High Rate, and High Cyclability Hybrid Electrical Energy Storage. *Chem. Mater.* **2012**, *24* (12), 2382−2390.
(64) Liang, W.; Poon, R.; Zhitomirsky, I. Zn-doped FeOOH-polypyrrole electrodes for supercapacitors. *Mater. Lett.* **2019**, *255*, No. 126542.
(65) Liang, W.; Zhitomirsky, I. MXene-polypyrrole electrodes for asymmetric supercapacitors. *Electrochim. Acta* **2022**, *406*, No. 139843.

https://doi.org/10.1021/acsaem.4c01204
ACS Appl. Energy Mater. 2024, 7, 5572−5581